Spectroscopic characteristics, magnetic properties and fluorescence dynamics of Tm^{3+} in YVO_4 crystal

1997 J. Phys.: Condens. Matter 9 7981

(http://iopscience.iop.org/0953-8984/9/38/006)

J. Phys.: Condens. Matter **9** (1997) 7981–7997. Printed in the UK PII: S0953-8984(97)84030-1

Spectroscopic characteristics, magnetic properties and fluorescence dynamics of Tm^{3+} in YVO_4 crystal

Chen Xueyuan† and Luo Zundu†‡

† Fujian Institute of Research on the Structure of Matter, Chinese Academy of Sciences, Fuzhou, Fujian 350002, People's Republic of China

‡ China Centre of Advance Science and Technology (World Laboratory), PO Box 8730, Beijing 100080, People's Republic of China

Received 7 May 1997

Abstract. Based on the analysis of the group-chain scheme, the crystal-field-level fitting has been carried out for Tm^{3+}:YVO_4, in which the Tm^{3+} ions occupy D_{2d} site symmetry positions. The RMS of energy-level fitting is 7.00 cm^{-1}. The wavefunctions obtained were used to the study of magnetic, thermal and spectroscopic properties of the crystal. The calculated *g*-factors confirm Karayianis' partial *g*-sum rule. The temperature dependence of Schottky specific heat and magnetic susceptibility agrees well with the experimental data. Using the Judd–Ofelt parameter analysis, the Ω_λ parameters are fitted to the absorption spectra with $\Omega_2 = 7.85$, $\Omega_4 = 4.74$, and $\Omega_6 = 0.071$ (in 10^{-20} cm^2). Considering the radiative, nonradiative transition and cross-relaxation ($^3H_4$, $^3H_6 \rightarrow 2\,^3F_4$) in Tm^{3+}:YVO_4, one set of rate equations is established to study the fluorescence dynamics. The relation between the ion's population density in the excited state and the doped ion concentration is discussed, and some useful inferences are drawn.

1. Introduction

Tm^{3+}-ion-doped laser crystals have been studied intensively as laser diode (LD) pumped tunable lasers near the 2000 nm wavelength region, and they are promising candidates for medical applications and remote sensing applications [1, 2]. It is reported that this type of laser device may be used as a light source for windshearing measurements or water vapour monitoring [3, 4]. Of the Tm^{3+}-doped crystals, Tm^{3+}:YVO_4 had not been investigated so much as the others in spite of its attractive features. For example, this crystal has a smoother and more intense absorption profile for the pump band which offers advantages for LD pumping, the peak of the pump band is shifted to a longer wavelength where high-power LD operates more efficiently, and it has strong birefringence which should facilitate the polarizing and *Q*-switch of the laser's output [5]. Experimental and calculated energy levels of Tm^{3+}:YVO_4 have been reported by Knoll [6] and Wortman *et al* [7]. The crystal-field (CF) parameters of Tm^{3+}:YVO_4 were used to find the temperature variation of Schottky specific heat and paramagnetic susceptibility by Kumar *et al* [8]. In recent years, Saito *et al* [5], Ohta *et al* [9, 10] and Henssen *et al* [11] have achieved its laser output near 2000 nm pumped by LD and carried out some spectroscopic measurements. It is important to study the detailed structures of the energy levels and the excitation kinetics in order to improve the laser efficiency.

In previous work, the energy levels and spectroscopic properties of NAB, NYAB [12], Nd^{3+}:YVO_4 [13], Er^{3+}:$LiYF_4$ [14] and Tm^{3+}:LiYF4 [15] have been investigated using the

0953-8984/97/387981+17$19.50

crystal-field analysis. The same method, namely, the group-chain scheme plus a constraint condition by the ratios of CF parameters, can also be applied to the study of Tm^{3+}:YVO_4. Utilizing the fitting wavefunctions, we can calculate the spectroscopic splitting g-factors, Schottky specific heat and paramagnetic susceptibility. In addition, Judd–Ofelt parameter analysis of the absorption spectra is presented and a rate equation model is established to describe the fluorescence dynamics of Tm^{3+} ions in YVO_4. All the results are discussed and compared with the data published by others.

2. Group-chain scheme analysis

The site symmetry of Tm^{3+} in YVO_4 is D_{2d}. Consider the group chain $O_3 \supset O_h \supset T_d \supset D_{2d}$; the detailed CF Hamiltonian can be expressed in Butler's notation

$$H_{cf} = C^{2+}_{2+2}b^{2+}_{2+2} + C^{4+}_{0+0}b^{4+}_{0+0} + C^{4+}_{2+2}b^{4+}_{2+2} + C^{6+}_{0+0}b^{6+}_{0+0} + C^{6+}_{2+2}b^{6+}_{2+2}. \tag{1}$$

Here $b^k_{\mu\nu}$ are the basis functions of the group chain $O_3 \supset O_h \supset T_d \supset D_{2d}$ and are identical to $|k\mu\nu 0\rangle$ in [16]; $C^k_{\mu\nu}$ are the expansion coefficients of H_{cf} by these bases; and symbol $+$ denotes that the representation belongs to the even-parity representation. Because all the basis functions belong to the 0 representation of D_{2d}, the index 0 for the D_{2d} group has been omitted.

The wavefunctions of all Stark levels can be expressed as

$$\Psi = \sum_{aa_1a_2a_3} C^a_{a_1a_2a_3}|aa_1a_2a_3\rangle. \tag{2}$$

The matrix elements of the CF Hamiltonian can be calculated by means of the Wigner–Eckart theorem and the factorization lemma of the $3jm$ factors.

$$\langle aa_1a_2a_3|H_{cf}|bb_1b_2b_3\rangle = \sum_{k\mu\nu} C^k_{\mu\nu}\begin{pmatrix} a \\ a_1 \end{pmatrix}\begin{pmatrix} a_1 \\ a_2 \end{pmatrix}\begin{pmatrix} a_2 \\ a_3 \end{pmatrix} \times \sum_{rr_1r_2r_3}\begin{pmatrix} a^* & k & b \\ a^*_1 & \mu & b_1 \end{pmatrix}_r \begin{pmatrix} a^*_1 & \mu & b_1 \\ a^*_2 & \nu & b_2 \end{pmatrix}_{r_1}\begin{pmatrix} a^*_2 & \nu & b_2 \\ a^*_3 & 0 & b_3 \end{pmatrix}_{r_2}\begin{pmatrix} r_2 \\ r_3 \end{pmatrix}\langle a\|b^k\|b\rangle \tag{3}$$

$$\langle a\|b^k\|b\rangle = \langle \mathrm{f}^n SLa\|U^{(k)}\|\mathrm{f}^n S'L'b\rangle\langle 4\mathrm{f}\|C^{(k)}\|4\mathrm{f}\rangle. \tag{4}$$

The reduced matrix elements (RME) $\langle f^n SLa\|U^{(k)}\|f^n S'L'b\rangle$ were calculated under the intermediate-coupling approximation by Pappalardo [17]. All the $2jm$ and $3jm$ factors can be found from [16]. The energy-level fitting is performed by two steps instead of by diagonalizing a combined spin–orbit and CF Hamiltonian. First, free-ion wavefunctions in a Russell–Saunders basis of J states are obtained by diagonalizing a Hamiltonian containing the Coulomb and spin–orbit interactions, and thus we can compute the RME of $U^{(k)}(k = 2, 4, 6)$ between all of the intermediate-coupled wavefunctions. Second, matrices (such as 10×10 of $^3H_6$, 7×7 of $^3F_4$ etc) representing the CF interaction are diagonalized simultaneously for $^{2S+1}L_J$ states, which have experimental data of energy levels, and the CF parameters are determined in a least-squares fit to the data. Here we assume that the centres of the gravity of J-multiplets are invariant even in the CF interaction, neglecting the effect of J-mixing in Tm^{3+}:YVO_4.

On the basis of the group–subgroup chain $O_3 \supset O_h \supset T_d \supset D_{2d}$, the wavefunctions of the $4f^{12}$ configuration in Tm^{3+} at the D_{2d} symmetry position are expressed as linear combinations of the bases $|\mathrm{f}^n SLJ\mu\nu\xi\rangle$, where μ, ν and ξ are the irreducible representations of O_h, T_d and D_{2d} respectively. The detailed matrix elements of all the terms can be

obtained from (3). The conventional CF parameters are calculated by the simple point-charge model. Consider the shielding factors of $5s^25p^6$ shells and the scaling parameters of the bare Hartree–Fock wavefunction [18],

$$B_{nm} = \rho_n A_{nm}. \tag{5}$$

With Tm^{3+}

$$\rho_2 = 0.1722 \qquad \rho_4 = 0.4053 \qquad \rho_6 = 0.9649.$$

A_{nm} is the result of the lattice sum. Using the conversion relationship between the conventional CF parameters and group-chain parameters [14], the initial values and r_0, r_1, the ratios of the same rank of group-chain parameters can be obtained, which are listed in tables 1 and 2. Note that

$$r_0 = C^{4+}_{2^+2}/C^{4+}_{0^+0} \qquad r_1 = C^{6+}_{2^+2}/C^{6+}_{0^+0}. \tag{6}$$

Table 1. CF parameters B_{nm} for Tm^{3+}:YVO_4 (in cm^{-1}).

B_{20}	B_{40}	B_{44}	B_{60}	B_{64}	Reference
290	980	2921	−846	−79	point-charge model
−132	377	898	−521	−52	[6]
−175	337	832	−612	−50	[7]
−173	341	830	−604	−55	fitting results

Table 2. Group-chain parameters and constraint ratios (in cm^{-1}).

$C^{2+}_{2^+2}$	$C^{4+}_{0^+0}$	$C^{4+}_{2^+2}$	$C^{6+}_{0^+0}$	$C^{6+}_{2^+2}$	r_0	r_1	Reference
−290	3415	−2522	194	−831	−0.74	−4.28	point-charge model
173	1018	−676	140	−593	−0.66	−4.23	fitting results

Using the ratios listed in table 2 as constraints in the least-squares fit, and adjusting the ratios to minimize the RMS deviation of the energy levels, the initial and final k-even parameters $C^k_{\mu\nu}$ (cm^{-1}) and the corresponding ratios can be obtained and given in table 2. Comparison of the experimental and fitting energy levels, with the group attributes of Stark sublevels, is shown in table 3. There are 43 levels with the greatest experimental confidence in this fit, giving a final RMS of 7.00 cm^{-1}. Comparing with the results of Wortman *et al* [7] (RMS = 10.6 cm^{-1}), we can see that the calculated eigenvalues agree better with the experimental energy levels. The wavefunctions of the Stark levels of total 11 terms are normalized and listed in order of increasing energy in the appendix. In the case of the D_{2d} group, Butler's notation 0, $\tilde{0}$, 2, $\tilde{2}$ and 1 correspond to Γ_1, Γ_2, Γ_3, Γ_4 and Γ_5 respectively, of Bethe's notation.

3. The Zeeman interaction, Schottky specific heat and magnetic susceptibility

Previously we have reported the theoretical calculation of the g-tensor of the ground and excited states in Er^{3+}:$LiYF_4$, Tm^{3+}:$LiYF_4$ [14, 15], on the basis of the group-chain scheme analysis. The detailed derivation of the formula of the g-factor is also presented there. In Tm^{3+}:YVO_4, all $g_\perp$ values of the Stark levels belonging to the Γ_5 representation are zero.

Only magnetic field H along the crystal z axis is to be considered. The calculated and experimental $g_\parallel$ values are listed in table 3. The $g_\parallel$ value of the ground state (9.41) agrees with the experiment (9.96) and Wortman's result (9.43). In order to confirm the reliability of the proposed method, we may sum all the g-factors over levels belonging to the Γ_5 irreducible representation of a particular $^{2S+1}L_J$ state to check the partial g-sums rule [19]. The sums are compared with theoretical values and Wortman's in table 4. It shows that the present results are in better agreement with the partial g-sums rule than Wortman's.

Another two interesting phenomena caused by the CF splitting are the Schottky anomaly and magnetic anisotropy. The molar Schottky specific heat (C_S) is calculated by the following equation:

$$C_S = \frac{Nk}{Z^2}\left[Z\sum_{i=1}^{n}\left(\frac{E_i^0}{kT}\right)^2 g_i \exp\left(-\frac{E_i^0}{kT}\right) - \left\{\sum_{i=1}^{n}\left(\frac{E_i^0}{kT}\right) g_i \exp\left(-\frac{E_i^0}{kT}\right)\right\}^2\right] \tag{7}$$

where E_i^0, g_i denotes the zeroth-order energy eigenvalue of the ith level and the degeneracy, respectively; $Z = \sum_{i=1}^{n} g_i \exp(-E_i^0/kT)$.

The molar magnetic susceptibility χ is given by the Van Vleck formulation:

$$\chi = \frac{N}{Z}\sum_{i=1}^{n}\left[\frac{(E_i^1)^2}{kT} - 2E_i^2\right]\exp(-E_i^0/kT) \tag{8}$$

where E_i^1, E_i^2 are the first- and second-order perturbation energy eigenvalues corresponding to magnetic field H parallel or perpendicular to the crystal z axis.

$$E_i^1 = \mu_B\langle\psi_i|\boldsymbol{L} + 2\boldsymbol{S}|\psi_i\rangle \tag{9}$$

$$E_i^2 = \mu_B^2\sum_{j\neq i}\frac{|\langle\psi_i|\boldsymbol{L} + 2\boldsymbol{S}|\psi_j\rangle|^2}{E_i^0 - E_j^0} \tag{10}$$

where ψ_i is the wavefunction of the Stark level listed in the appendix. The principal magnetic susceptibility $\chi_\parallel$ and $\chi_\perp$ and the anisotropy $\Delta\chi = \chi_\parallel - \chi_\perp$ are obtained from (8). The effective magnetic dipole moment $\mu_{eff} = (3kT\bar{\chi}/N)^{1/2}$, where $\bar{\chi} = (\chi_\parallel + 2\chi_\perp)/3$ is the mean molar magnetic susceptibility. The CF effect of the excited terms on the ground state is neglected in the following calculation. On the basis of the perturbation technique and the proposed method, E_i^1, E_i^2 are computed and shown in table 5. The temperature dependences of C_S, $\bar{\chi}T$, μ_{eff} and $\Delta\chi$ are plotted in figures 1–3.

Figure 1 exhibits a comparatively broad peak at 86 K with the magnitude 7.25 J mol^{-1} K^{-1}. The extra entropy associated with the Schottky anomaly estimated from the specific heat curve up to 400 K is 14.45 J mol^{-1} K^{-1}. The value agrees fairly well with the free ion value (15.55) determined from the entropy expression for a system with doublet ground state, $S = R\ln(J + 1/2)$.

From figures 2 and 3, it is evident that $\chi_\parallel$ is always larger than $\chi_\perp$. The values of $\bar{\chi}T$ and μ_{eff} do not change more than 10% and 6% from 90 K to 400 K. The effective magnetic moment at room temperature comes out to be 7.50 μ_B, which agrees well with the free ion magnitude 7.56 μ_B for Tm^{3+} ion obtained from Hund's formula as well as the experimental value 7.61 μ_B for Tm metal [20]. The mean magnetic susceptibility for temperature above 10 K obeys Curie–Weiss law $\bar{\chi} = C/(T+\theta)$. The Curie constant ($C$) and Curie temperature (θ) come out to be 7.35 erg K G^{-2} mol^{-1} and 13.41 K respectively. Cooke *et al* [21] had measured magnetic susceptibility on $TmVO_4$ at temperatures in the range 0.5–4.2 K with $\chi_\parallel = 2.99$ at 3 K, 2.33 at 4 K and $\chi_\perp = 0.095$ at 4 K (in erg G^{-2} mol^{-1}), while our calculation on Tm^{3+}:YVO_4 presents the results with $\chi_\parallel = 2.78$ at 3 K, 2.08 at 4 K and $\chi_\perp = 0.150$ at 4 K. The agreement between them indicates that the method proposed may

Table 3. Comparison of the observed and calculated energy levels and g-factors of Tm^{3+} in YVO_4.

J		Energy (cm^{-1})		$g_\parallel$		
Multiplet	Γ	Experimental[a]	Theoretical[b]	Experimental[a]	Theoretical[b]	Theoretical[c]
$^3H_6$	5	0	2	9.96	9.41	9.43
	1	54*	33			
	4	119	111			
	5	138	143		−0.21	−0.25
	2	158	148			
	3	192	184			
	4	208	220			
	1	—	302			
	5	332	339		−2.21	−2.15
	3	—	367			
$^3F_4$	4	5550	5558			
	5	5655	5661		−2.63	−2.41
	1	5723	5719			
	2	5775	5775			
	3	5825*	5794			
	5	5860	5862		−2.37	−2.09
	1	5879	5890			
$^3H_5$	2	8204	8209			
	1	8232*	8 264			
	5	8268	8266		−0.38	0.14
	3	8296	8297			
	5	8338	8335		6.53	5.97
	2	8440	8435			
	5	—	8 461		0.05	0
	4	8491	8478			
$^3H_4$	5	12 523	12 525	−4.84	−3.92	−4.61
	1	12 563	12 558			
	2	12 633	12 646			
	4	12 662	12 659			
	1	12 705	12 698			
	5	12 704	12 699		0.72	0.79
	3	12 774	12 783			
$^3F_3$	5	14 411	14 410	−0.64	2.01	1.23
	3	14 453	14 436			
	5	14 453	14 460	−6.04	−6.35	−5.49
	4	14 459	14 467			
	2	14 475	14 472			
$^3F_2$	3	15 007	15 015			
	1	15 018	15 022			
	5	15 069	15 064	1.84	1.33	1.47
	4	15 147	15 144			
$^1G_4$	4	20 938*	20 960			
	5	21 102	21 100	−2.68	−2.49	−2.37
	1	21 167	21 166			
	2	21 234	21 237			
	3	21 306	21 306			

Table 3. (Continued)

J Multiplet	Γ	Energy (cm^{-1}) Experimental[a]	Theoretical[b]	$g_\parallel$ Experimental[a]	Theoretical[b]	Theoretical[c]
$^1G_4$	5	—	21 397		−1.51	−1.50
	1	21 459*	21 437			
$^1D_2$	1	27 735	27 731			
	5	27 736	27 734	1.19	2	2.31
	4	27 753	27 757			
	3	27 789	27 795			
$^1I_6$	3		34 790			
	4		34 821			
	5		34 858		0.53	0.46
	1		34 864			
	3		34 917			
	5		35 041		5.36	5.40
	2		35 063			
	4		35 233			
	5		35 249		0.11	0.14
	1		35 264			
$^3P_1$	5		35 781		3	3.02
	2		35 833			
$^3P_2$	3		37 691			
	1		37 720			
	5		37 806		3	2.51
	4		37 967			

[a]Knoll's spectra [6].
[b]Present results.
[c]Wortman's crystal-field-levels fit [7].
*Levels excluded from the final fit.

predict magnetic properties of rare-earth-doped crystals at low temperature. The magnetic anisotropy $\Delta\chi$ increases sharply with the fall of temperature, which is in accordance with the low symmetry of the CF in Tm^{3+}:YVO_4.

The curves depicted here are in agreement with Kumar's [8] in spite of the different methods adopted in both calculations. Therefore it is reasonable to conclude that the method introduced is effective and the CF parameters presented are reliable.

4. Judd–Ofelt parameter analysis

Judd–Ofelt parameter calculation has become the most popular method in analysing optical transition properties of rare-earth ions. According to this theory, the electric-dipole radiative transition rate $A(\alpha J, \alpha' J')$ can be expressed as follows:

$$A(\alpha J, \alpha' J') = \frac{64\pi^4 e^2}{3h(2J+1)\lambda^3}\frac{n(n^2+2)}{9}S(\Psi J, \Psi' J') \tag{11}$$

Table 4. Comparison of partial g-sums with theoretical values for the terms of Tm^{3+} in YVO_4.

	Γ_5 (1)		
J	$\mu = 1$[a]	Tm^{3+}:YVO_4[b]	Tm^{3+}:YVO_4[c]
$^3H_6$	7.00	6.99	7.03
$^3F_4$	−5.00	−5.00	−4.50
$^3H_5$	6.20	6.20	6.11
$^3H_4$	−3.20	−3.20	−3.82
$^3F_3$	−4.33	−4.34	−4.26
$^3F_2$	1.33	1.33	1.47
$^1G_4$	−4.00	−4.00	−3.87
$^1D_2$	2.00	2.00	2.31
$^1I_6$	6.00	6.00	6.00
$^3P_1$	3.00	3.00	3.02
$^3P_2$	3.00	3.00	2.51

[a]Theoretical values [19].
[b]Present results,
[c]Wortman's results [7].
[μ]Crystal quantum number.

Table 5. The Zeeman splitting of Stark sublevels of $^3H_6$ in Tm^{3+}:YVO_4.

	Group attribute		$\chi_\parallel$		$\chi_\perp$	
$^3H_6$	Γ	E_i^0	E_i^1 (μ_B)	$E_i^2(\mu_B^2 \times 10^{15})$	$E_i^1(\mu_B)$	$E_i^2(\mu_B^2 \times 10^{15})$
(a)	5	2	± 4.705	−0.1965	0	−1.4456
(b)	1	33	0	−0.5470	0	1.9251
(c)	4	111	0	−0.9732	0	−1.8017
(d)	5	143	± 0.105	0.0258	0	−4.7217
(e)	2	148	0	0.2460	0	11.2581
(f)	3	184	0	−3.6250	0	0.1657
(g)	4	220	0	4.3330	0	0.5554
(h)	1	302	0	0.3020	0	−2.7574
(i)	5	339	± 1.105	0.1706	0	−0.6874
(j)	3	367	0	0.2650	0	4.3642

where the line-strength $S(\Psi J, \Psi' J')$ is described with the reduced matrix element and the intensity parameters Ω_λ, that is,

$$S(\Psi J, \Psi' J') = \sum_{\lambda=2,4,6} \Omega_\lambda |\langle \Psi J \| U^{(\lambda)} \| \Psi' J' \rangle|^2. \tag{12}$$

$\Omega_\lambda$are usually fitted to the absorption spectra by

$$\int_0^\infty k(\lambda)\, \mathrm{d}\lambda = \rho \frac{8\pi^3 \lambda e^2}{3ch(2J+1)} \frac{(n^2+2)^2}{9n} S(\Psi J, \Psi' J') \tag{13}$$

where $k(\lambda)$, ρ and n are the absorbance, the Tm^{3+} ion number density and refractive index, respectively. Ohta *et al* [9] has fitted the Ω_λ-parameters to the experimental σ and π absorption spectra using the Judd–Ofelt method. Nevertheless, there exist some puzzles in their calculation. As we know, (11) was originally derived in the case of isotropic media. In obtaining this equation, it was assumed that the radiative emission is distributed over a 4π solid angle. Hence $S(\Psi J, \Psi' J')$ in (11) should be a spatially averaged line-strength

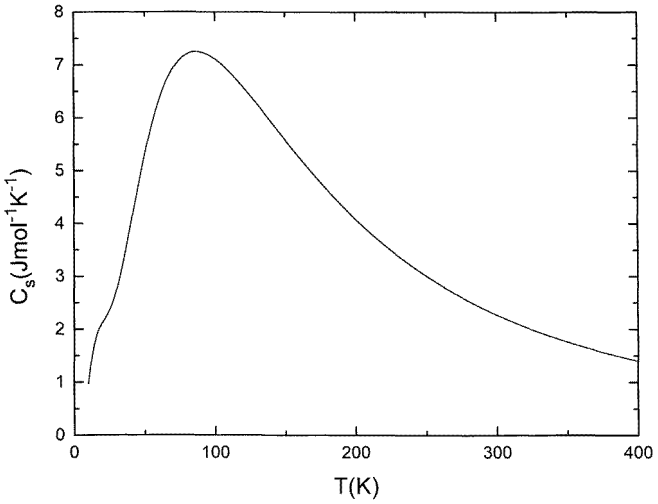

Figure 1. Temperature variation of Schottky specific heat for Tm^{3+}:YVO_4.

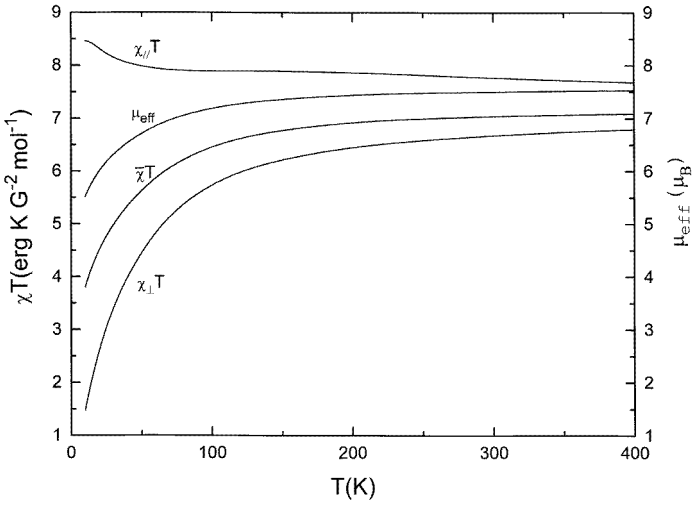

Figure 2. Temperature variation of principal susceptibilities for Tm^{3+}:YVO_4.

when one use it in the cases of anisotropic media, and in order to combine it with (13), it is necessary to use the spatially averaged absorbances [22]. As pointed out by us [23], the corresponding effective Judd–Ofelt parameter should be $\Omega_{eff} = (\Omega_\pi + 2\Omega_\sigma)/3$ instead of $\Omega_{eff} = (\Omega_\pi + 2\Omega_\sigma)$ in [9]. In fact, the calculated radiative lifetime of $^3F_4$ using their derived parameters is 695 μs, which is even shorter than the measured fluorescence lifetime 800 μs [9]. We believe it is unreasonable. Using the measured polarized spectra [9] and TPM method proposed in [23], we refit the Ω_λ-parameters. The results are shown in tables 6–8. During the least-squares fit process, Ω_6 first comes out to be negative which has no physical meaning. Therefore a positive value for Ω_6 as constraint condition was put in the fit to search for the minimum RMS. Table 6 shows the experimental and calculated

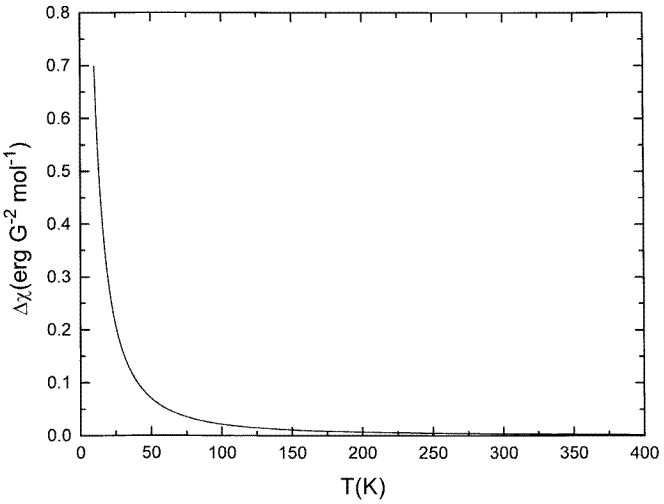

Figure 3. Temperature variation of magnetic anisotropy for Tm^{3+}:YVO_4.

Table 6. Measured absorbances and the line-strengths obtained from the experiment and from the least-squares fit.

Transitions $^3H_6 \rightarrow$	$\bar{\lambda}$ (nm)	n	Absorbance Γ (nm cm^{-1})	Line-strength (10^{-20} cm^2)	
				Experimental	This work
$^3F_4$ (π)	1738.1	2.149	1280.7	7.341	7.046
(σ)		1.946	1266.0	8.595	7.878
$^3H_5$ (π)	1218.9	2.159	201.0	1.629	1.809
(σ)		1.953	119.0	1.145	2.074
$^3H_4$ (π)	790.9	2.187	141.4	1.726	2.244
(σ)		1.973	101.9	1.487	2.591
$^3F_3$ (π)	692.3	2.202	81.3	1.119	1.416
(σ)		1.984	69.0	1.139	1.631
$^3F_2$ (π)	663.9	2.208	0	0	0
(σ)		1.988	1.6	0.027	0.027
$^1G_4$ (π)	477.6	2.282	23.7	0.443	0.696
(σ)		2.040	21.5	0.491	0.776

line-strength of each absorption band including σ- and π-polarization. The reduced matrix elements for Tm^{3+} were taken from Pappalardo's data [17]. The refractive indices are calculated according to the Sellmeier dispersion equation of Tm^{3+}:YVO_4 [24]. Table 7 shows the summary of the fitted Ω_λ. The calculated radiative transition rates from the excited manifolds, by substituting the obtained Ω_λ into (11) and (12), are listed in table 8.

As shown in table 8, the calculated radiative lifetime of $^3F_4$ is 1165 μs. In comparison to the fluorescence lifetime 800 μs [9], we can give the quantum efficiency η, $\eta = 69\%$. This result is reasonable and in consistent with the physical reality. The calculated radiative lifetime of $^3H_4$ is 262 μs, compared with the fluorescence lifetime 48 μs [9]. The effect of the nonradiative cross-relaxation process ($^3H_4$, $^3H_6 \rightarrow 2\,^3F_4$) is responsible for this difference, which we shall discuss in the next section.

Table 7. The fitted Ω_λ parameters (in 10^{-20} cm^2).

	π-spectrum	σ-spectrum	Averaged unpolarized spectrum ($\bar{\Omega}_\lambda$)	[9]
$\Omega_\lambda(\lambda = 2, 4, 6)$	7.19, 4.48, 0	8.17, 4.87, 0.11	7.85, 4.74, 0.071	13.0, 6.0, 0.082

Table 8. The calculated radiative transition rates and branching ratios from the excited manifolds of Tm^{3+}:YVO_4.

Transition	$\bar{\lambda}$ (nm)	Transition rate (s^{-1})	Total transition rates (s^{-1})	Radiative lifetime (μs)	Branching ratios β
$^3F_4 \rightarrow {}^3H_6$	1800	859	859	1165	1
$^3H_5 \rightarrow {}^3F_4$	3857	13	606	1650	2.1%
$\rightarrow {}^3H_6$	1224	593			97.9%
$^3H_4 \rightarrow {}^3H_5$	2327	124	3823	262	3.3%
$\rightarrow {}^3F_4$	1451	360			9.4%
$\rightarrow {}^3H_6$	802	3338			87.3%

The peak cross-section of the transition $^3F_4 \rightarrow {}^3H_6$ ($\lambda = 1800$ nm) can be estimated by

$$\sigma_{ij} = \frac{A_{ij}\lambda^2}{4\pi^2 n^2 \Delta\nu} = \frac{A_{ij}\lambda^4}{4cn^2\Delta\lambda} \tag{14}$$

where the line shape of the fluorescence spectrum is assumed to be Lorentzian; $\Delta\lambda$ is the bandwidth at full width at half-maximum (FWHM) of the transition, which is 117 nm roughly estimated from the fluorescence spectrum [5]. Finally σ comes out to be 1.61×10^{-20} cm^2. The result agrees well with the experimental cross-section of the π spectrum of transition $^3F_4 \rightarrow {}^3H_6$ at 1800 nm, i.e., 1.6×10^{-20} cm^2 [10], which indicates the reliability of the calculated intensity parameters.

5. Fluorescence dynamics of Tm^{3+} ions in YVO_4 crystal

The excitation process of Tm^{3+} ions is shown in figure 4. The $^3H_6 \rightarrow {}^3H_4$ transition near 800 nm corresponding to the AlGaAs LD wavelength is used for the pumping. It is assumed that the $^3H_5 \rightarrow {}^3F_4$ transition and the cross-relaxation ($^3H_4$, $^3H_6 \rightarrow 2\,{}^3F_4$) are the only effective nonradiative transitions, and the up-conversion process is negligible, according to Henssen *et al* [11]. In this paper, the reasonable lifetime for $^3H_5$ is taken to be 1 μs. N_1, N_2, N_3 and N_4 are the Tm^{3+} ion population densities for $^3H_6$, $^3F_4$, $^3H_5$ and $^3H_4$ respectively. A_{ij} in figure 4 is the corresponding radiative transition rate between terms and is listed in table 8. P is the cross-relaxation rate for $^3H_4$, $^3H_6 \rightarrow 2\,{}^3F_4$.

According to Dexter's theory [25], the cross-relaxation is caused dominantly by the dipole–dipole and dipole–quadrupole interactions between Tm^{3+} ions in YVO_4. Hence P can be expressed as follows:

$$P = P_{dd} + P_{dq} \tag{15}$$

$$P_{dd} = \frac{8\pi^2 e^2 S}{3h^2 c g_1 g_4 R^6}\left(\frac{n^2+2}{3n}\right)^4 \sum_{\lambda=2,4,6} \Omega_\lambda |\langle {}^3H_4 \| U^{(\lambda)} \| {}^3F_4\rangle|^2 \sum_{\lambda=2,4,6} \Omega_\lambda |\langle {}^3H_6 \| U^{(\lambda)} \| {}^3F_4\rangle|^2 \tag{16}$$

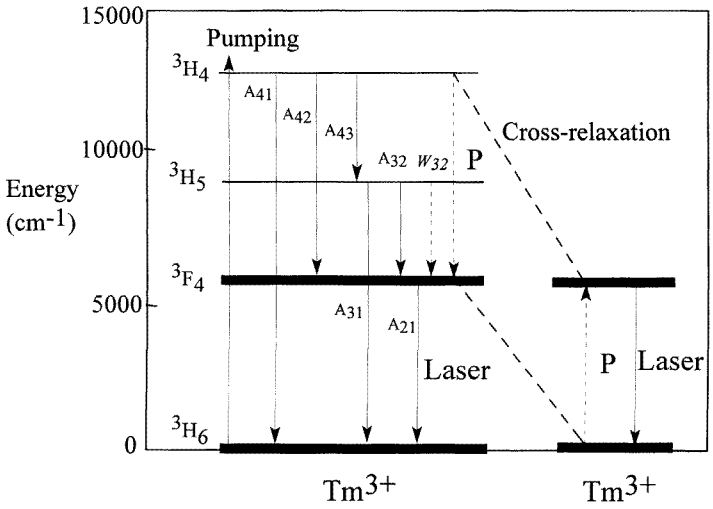

Figure 4. Energy-level diagram of Tm^{3+} ions in a crystal. The arrows with the solid lines show the radiative transitions and those with the dotted lines denote the nonradiative transitions.

$$P_{dq} = \frac{9 \times 1.266\pi^2 e^4 S}{h^2 c g_1 g_4 R^8} \left(\frac{n^2+2}{3n}\right)^4 \frac{4}{9} [\langle 4f \| C^{(2)} \| 4f \rangle \langle r^2 \rangle \langle {}^3H_4 \| U^{(2)} \| {}^3F_4 \rangle]^2 \times \sum_{\lambda=2,4,6} \Omega_\lambda |\langle {}^3H_6 \| U^{(\lambda)} \| {}^3F_4 \rangle|^2 \tag{17}$$

where S is the integral of the line shape overlap between the absorption ${}^3H_6 \rightarrow {}^3F_4$ and emission ${}^3H_4 \rightarrow {}^3F_4$, and is approximately $1/\pi\Delta\tilde{\nu}$ when the line shapes are assumed to be Lorentzian; $\Delta\tilde{\nu}$ (cm^{-1}) is set to be the larger bandwidth at FWHM between the absorption and emission transitions. Here $\Delta\tilde{\nu}$ should be the line width of the absorption transition, and finally S is calculated to be about 8.82×10^{-4} cm. g_1 and g_4 are the degeneracies for ${}^3H_6$ and ${}^3H_4$ respectively, with $g_1 = 13$, $g_4 = 9$. The reduced matrix elements for Tm^{3+} are given in [17]. Ω_λ are listed in table 7. The refractive index n is averaged to be 2.015. The value of $\langle r^2 \rangle$ is interpolated to be 0.64 au (atomic unit) according to Freeman and Watson [26]. R is the distance between the doped ions. Supposing x is the relative concentration (in atomic percentage) of the doped ions, it is easily shown that $1/R^3$ is proportional to x, and $1/R^3 = x/R_0^3$, where R_0 is the distance to the nearest Tm^{3+} ions in $TmVO_4$. Also $N = N_0 x$, where N is the doped ion number density and N_0 is the total cation number density in YVO_4 that can be substituted by Tm^{3+}. From the crystal structure of $TmVO_4$ [27], we get: $R_0 = 3.865$ Å, $N_0 = 1.279 \times 10^{22}$ cm^{-3}. By using all the data above, the cross- relaxation rate P should be:

$$P = 3.066 \times 10^6 x^2 + 1.867 \times 10^7 x^{8/3} \ (s^{-1}). \tag{18}$$

Considering the radiative, nonradiative transition and cross-relaxation in Tm^{3+}:YVO_4,

we may establish the following set of rate equations to study its fluorescence dynamics.

$$\begin{cases} \dfrac{\mathrm{d}N_4}{\mathrm{d}t} = N_1 W - N_4(A_{41} + A_{42} + A_{43}) - N_4 P \\ \dfrac{\mathrm{d}N_3}{\mathrm{d}t} = N_4 A_{43} - N_3(A_{31} + A_{32} + \omega_{32}) \\ \dfrac{\mathrm{d}N_2}{\mathrm{d}t} = N_4 A_{42} + N_3(A_{32} + \omega_{32}) - N_2 A_{21} + (N_1 + N_4)P \\ N = N_1 + N_2 + N_3 + N_4 \end{cases} \tag{19}$$

where W is the pumping rate for the absorption $^3\mathrm{H}_6 \rightarrow {}^3\mathrm{F}_4$. Being interested in the steady state, we assume $\mathrm{d}N_4/\mathrm{d}t = \mathrm{d}N_3/\mathrm{d}t = \mathrm{d}N_2/\mathrm{d}t = 0$. The solutions for the rate equations are:

$$\begin{cases} N_4 = \dfrac{A_{21} W \tau_3^{-1} N_0 x}{\tau_3^{-1}[(W + P + \tau_4^{-1})(A_{21} + P) + A_{42} W] + A_{43}(A_{21} + \tau_3^{-1})W} \\ N_3 = A_{43}\tau_3 N_4 \\ N_2 = \dfrac{P N_1 + \tau_3^{-1} N_3 + (A_{42} + P)N_4}{A_{21}} \\ N_1 = \dfrac{\tau_4^{-1} + P}{W} N_4 \end{cases} \tag{20}$$

where $\tau_3^{-1} = A_{31} + A_{32} + \omega_{32} \approx 10^6$ (s^{-1}), and $\tau_4^{-1} = A_{41} + A_{42} + A_{43}$. The relation between the relative population density (N_i/N_0) and the doped ion concentration x is depicted in figure 5(A)–(C) when $W = 10^2$, 10^3 and 10^4 s^{-1} respectively. The minimal doped ion concentrations in different pumping rates in order to achieve the minimal population inversion for the $^3\mathrm{F}_4 \rightarrow {}^3\mathrm{H}_6$ transition are listed in table 9, which can be seen to some extent as a measure of the pumping rate to reach laser oscillation.

Table 9. The minimal doped Tm^{3+} concentration in different pumping rates.

W (s^{-1})	1	10	100	1000	2000	5000	10000
Concentration (at.%)	1.5	~1.5	1.4	1.3	1.1	0.6	0.1

Due to multiphonon nonradiative transitions, the population of the $^3\mathrm{H}_5$ term is significantly quenched, i.e., N_3 is nearly zero and thus negligible, which is not depicted in figure 5. The existence of the maximum of N_1 as shown in figure 5 can be explained as follows. In the case of a certain pumping rate, when the doped concentration x is small, the ion numbers pumped into the $^3\mathrm{H}_4$ manifold are limited. The distance between Tm^{3+} ions in the lattice is so large that the ions' interactions are weak and hence the cross-relaxation rate is very small. This certainly leads to the increase of N_1 with the increase of x. Nevertheless, when x increases to some extent, the distance between ions will be shortened and the cross-relaxation rate will increase sharply, which quickly depletes the ions populating in $^3\mathrm{H}_4$ and ions in the ground state are simultaneously excited to $^3\mathrm{F}_4$. Then N_1 decreases with the further increase of x. As for the population of $^3\mathrm{F}_4$, we find it constantly increases with the increase of x. When x is larger than 5 at.%, almost all the ions populate the $^3\mathrm{F}_4$ term. From figure 5, we may conclude that the larger the doped concentration, the better the lasing of $^3\mathrm{F}_4 \rightarrow {}^3\mathrm{H}_6$ will be as long as it exceeds the minimal doped concentration. In addition, a useful inference can be drawn from table 9: even under low pumping rate, the

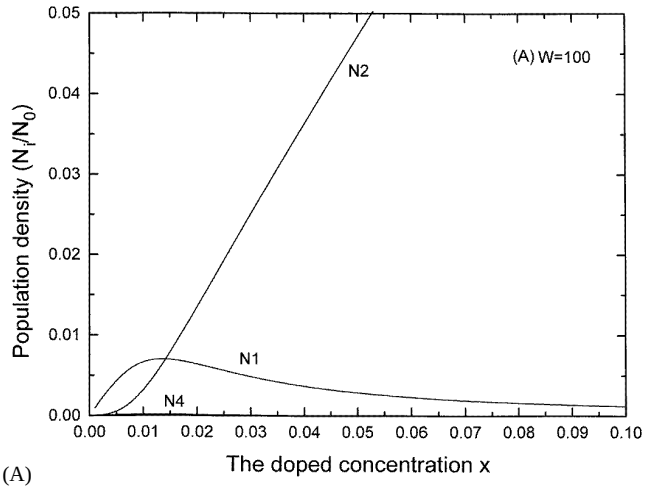

(A)

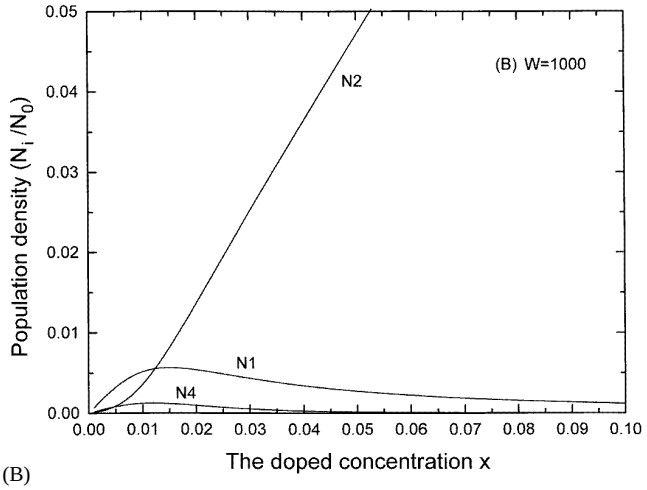

(B)

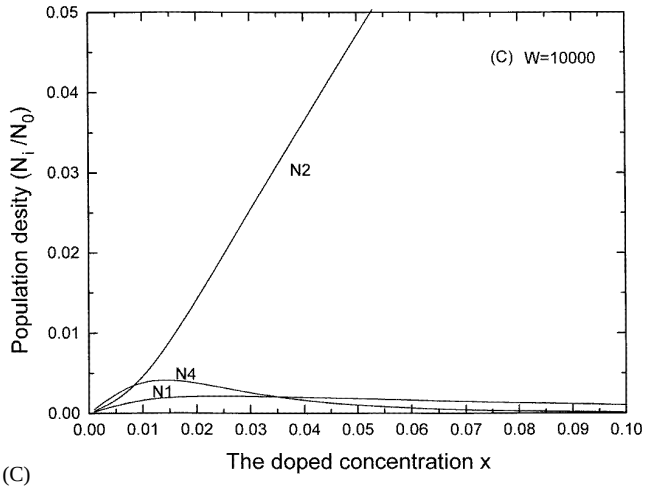

(C)

Figure 5. The relative population density N_i/N_0 in each manifold as a function of the doped concentration x of Tm^{3+} ions in YVO_4: (A) $W = 10^2$; (B) $W = 10^3$; (C) $W = 10^4$.

population inversion ($N_2 - N_1 > 0$) can be realized, which indicates the low-threshold and high-efficiency properties for the lasing of $^3F_4 \rightarrow {}^3H_6$.

The relationship between the fluorescent lifetime of $^3H_4$ and the doped concentration is discussed and shown in figure 6 (curve A)

$$\tau_{cal}^{-1} = \tau_{rad}^{-1} + P = \tau_4^{-1} + 3.066 \times 10^6 x^2 + 1.867 \times 10^7 x^{8/3}. \tag{21}$$

When $x = 5$ at.%, $\tau_{cal} = 56$ μs, which agrees well with the experimental value 48 μs [9]. According to Inokuti and Hirayama [28], the $^3H_4$ fluorescence decay curves for different Tm^{3+} concentrations obey the following relations:

$$\ln \frac{I(t)}{I(0)} = -\frac{t}{\tau_0} - \Gamma\left(1 - \frac{3}{s}\right)\frac{c}{c_0}\left(\frac{t}{\tau_0}\right)^{3/s} \tag{22}$$

where τ_0 is the intrinsic radiative lifetime; c and c_0 are the Tm^{3+} concentration and critical transfer concentration respectively. For the dipole–dipole energy transfer process, $s = 6$. When $I(t)/I(0) = 1/e$, $t = \tau$ and $c/c_0 = (\tau_0 P_{dd})^{1/2}$. (22) can be expressed as

$$\tau + (\pi^{1/2} P_{dd}^{1/2} \tau_0)\tau^{1/2} - \tau_0 = 0. \tag{23}$$

The lifetimes are calculated and shown in figure 6 (curve B). Comparison of curves A and B in figure 6 shows that two different methods in the calculation of the lifetime of $^3H_4$ are in moderate agreement.

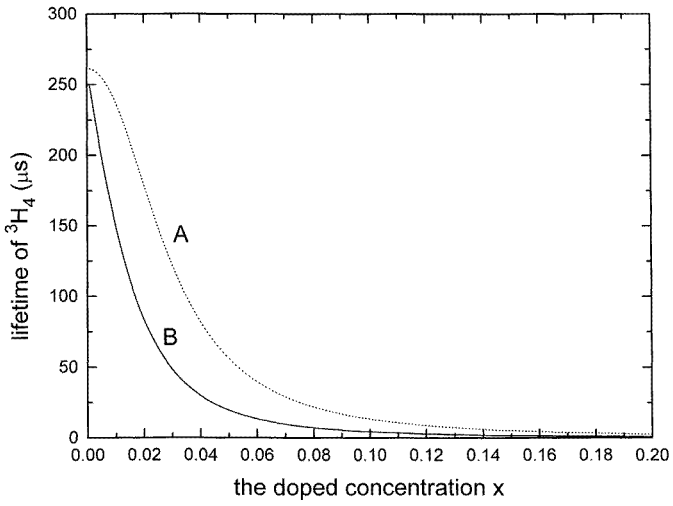

Figure 6. Fluorescence lifetime as a function of the doped Tm^{3+} concentration: (A) this work; (B) according to Inokuti's theory [28].

6. Conclusion

Group-chain scheme analysis has been carried out for Tm^{3+} ions of YVO_4 in D_{2d} low-symmetry sites, and by using the ratios calculated by the point-charge model as constraint condition, the CF energy level fitting is performed. With the aid of the least-squares fit programs, the CF parameters and the wavefunctions of Stark sublevels belonging to 11 terms with real physical meaning have been obtained. The RMS of the fit is 7.00 cm^{-1}.

On the basis of wavefunctions obtained, the g-factors of excited manifolds are calculated and compared with those of the experiment, which confirms the partial g-sums rule of Karayianis. Considering only the CF effect of the ground state $^3H_6$, the temperature dependence of Schottky specific heat, magnetic susceptibility and anisotropy are described and depicted for Tm^{3+}:YVO_4 from 10 to 400 K. The agreement with the experimental or theoretical results published by others shows that the method proposed is effective, and that the CF parameters are reliable.

Finally, we discuss the fluorescence dynamics of Tm^{3+} in YVO_4. Using the Judd–Ofelt parameter analysis and the measured absorption spectra by Ohta *et al* [9], we refit the Ω_λ parameters and present the results: $\Omega_2 = 7.85$, $\Omega_4 = 4.74$, $\Omega_6 = 0.071$ (10^{-20} cm^2). Considering the radiative, nonradiative transition and cross-relaxation ($^3H_4$, $^3H_6 \rightarrow 2^3F_4$) in Tm^{3+}:YVO_4, we establish one set of rate equations to study the fluorescence properties, such as the relation between the minimal doped concentration and pumping rate, the relations between the ion population density, the lifetime of $^3H_4$ and the Tm^{3+}-doped concentration respectively. When the doped ion concentration is 5 at.%, the calculated radiative lifetime of $^3F_4$ is 1165 μs and the fluorescence lifetime of $^3H_4$ is 56 μs, which shows agreement with the experimental fluorescence lifetime 800 μs and 48 μs respectively.

In brief, we have studied the energy structure, magnetic properties and fluorescence dynamics of the Tm^{3+}:YVO_4 crystal. Some of our results may be used as a guide to the development of a Tm^{3+}:YVO_4 laser, and the method introduced can be applied to the investigation of new laser and magnetic materials.

Appendix. Wavefunctions for the crystal-field energy levels in Tm^{3+}:YVO_4 ($O_3 \supset O_h \supset T_d \supset D_{2d}$)

$^3H_6$	(a)	$-0.8292\|6^+1^+11\rangle - 0.3978\|6^+\tilde{1}_0^+\tilde{1}1\rangle + 0.3927\|6^+\tilde{1}_1^+\tilde{1}1\rangle$	(Γ_5)
	(b)	$0.9394\|6^+0^+00\rangle - 0.3428\|6^+2^+20\rangle$	(Γ_1)
	(c)	$0.8119\|6^+\tilde{1}_0^+\tilde{1}\tilde{2}\rangle - 0.5838\|6^+\tilde{1}_1^+\tilde{1}\tilde{2}\rangle$	(Γ_4)
	(d)	$-0.4748\|6^+1^+11\rangle + 0.1305\|6^+\tilde{1}_0^+\tilde{1}1\rangle - 0.8704\|6^+\tilde{1}_1^+\tilde{1}1\rangle$	(Γ_5)
	(e)	$\|6^+1^+1\tilde{0}\rangle$	(Γ_2)
	(f)	$-0.6591\|6^+2^+22\rangle + 0.7521\|6^+\tilde{0}^+\tilde{0}2\rangle$	(Γ_3)
	(g)	$0.5838\|6^+\tilde{1}_0^+\tilde{1}\tilde{2}\rangle + 0.8119\|6^+\tilde{1}_1^+\tilde{1}\tilde{2}\rangle$	(Γ_4)
	(h)	$0.3428\|6^+0^+00\rangle + 0.9394\|6^+2^+20\rangle$	(Γ_1)
	(i)	$-0.2950\|6^+1^+11\rangle + 0.9082\|6^+\tilde{1}_0^+\tilde{1}1\rangle + 0.2970\|6^+\tilde{1}_1^+\tilde{1}1\rangle$	(Γ_5)
	(j)	$0.7521\|6^+2^+22\rangle + 0.6591\|6^+\tilde{0}^+\tilde{0}2\rangle$	(Γ_3)
$^3F_4$	(a)	$\|4^+\tilde{1}^+\tilde{1}\tilde{2}\rangle$	(Γ_4)
	(b)	$0.3992\|4^+1^+11\rangle + 0.9169\|4^+\tilde{1}^+\tilde{1}1\rangle$	(Γ_5)
	(c)	$-0.0924\|4^+0^+00\rangle + 0.9957\|4^+2^+20\rangle$	(Γ_1)
	(d)	$\|4^+1^+1\tilde{0}\rangle$	(Γ_2)
	(e)	$\|4^+2^+22\rangle$	(Γ_3)
	(f)	$-0.9169\|4^+1^+11\rangle + 0.3992\|4^+\tilde{1}^+\tilde{1}1\rangle$	(Γ_5)
	(g)	$0.9957\|4^+0^+00\rangle + 0.0924\|4^+2^+20\rangle$	(Γ_1)
$^3H_5$	(a)	$-0.9989\|5^+1_0^+1\tilde{0}\rangle - 0.0472\|5^+1_1^+1\tilde{0}\rangle$	(Γ_2)
	(b)	$\|5^+2^+20\rangle$	(Γ_1)
	(c)	$0.8785\|5^+1^+11\rangle - 0.0583\|5^+\tilde{1}_0^+\tilde{1}1\rangle + 0.4742\|5^+\tilde{1}_1^+\tilde{1}1\rangle$	(Γ_5)
	(d)	$\|5^+2^+22\rangle$	(Γ_3)
	(e)	$0.3438\|5^+1^+11\rangle - 0.6120\|5^+\tilde{1}_0^+\tilde{1}1\rangle - 0.7122\|5^+\tilde{1}_1^+\tilde{1}1\rangle$	(Γ_5)

	(f)	$-0.0472\|5^+1_0^+1\tilde{0}\rangle + 0.9989\|5^+1_1^+1\tilde{0}\rangle$	(Γ_2)
	(g)	$-0.3317\|5^+1^+11\rangle - 0.7887\|5^+\tilde{1}_0^+\tilde{1}1\rangle + 0.5176\|5^+\tilde{1}_1^+\tilde{1}1\rangle$	(Γ_5)
	(h)	$\|5^+\tilde{1}^+\tilde{1}\tilde{2}\rangle$	(Γ_4)
$^3H_4$	(a)	$0.0191\|4^+1^+11\rangle + 0.9998\|4^+\tilde{1}^+\tilde{1}1\rangle$	(Γ_5)
	(b)	$0.2089\|4^+0^+00\rangle + 0.9779\|4^+2^+20\rangle$	(Γ_1)
	(c)	$\|4^+1^+1\tilde{0}\rangle$	(Γ_2)
	(d)	$\|4^+\tilde{1}^+\tilde{1}\tilde{2}\rangle$	(Γ_4)
	(e)	$-0.9779\|4^+0^+00\rangle + 0.2089\|4^+2^+20\rangle$	(Γ_1)
	(f)	$-0.9998\|4^+1^+11\rangle + 0.0191\|4^+\tilde{1}^+\tilde{1}1\rangle$	(Γ_5)
	(g)	$\|4^+2^+22\rangle$	(Γ_3)
$^3F_3$	(a)	$0.5011\|3^+1^+11\rangle + 0.8654\|3^+\tilde{1}^+\tilde{1}1\rangle$	(Γ_5)
	(b)	$\|3^+\tilde{0}^+\tilde{0}2\rangle$	(Γ_3)
	(c)	$-0.8654\|3^+1^+11\rangle + 0.5011\|3^+\tilde{1}^+\tilde{1}1\rangle$	(Γ_5)
	(d)	$\|3^+\tilde{1}^+\tilde{1}\tilde{2}\rangle$	(Γ_4)
	(e)	$\|3^+1^+1\tilde{0}\rangle$	(Γ_2)
$^3F_2$	(a)	$\|2^+2^+22\rangle$	(Γ_3)
	(b)	$\|2^+2^+20\rangle$	(Γ_1)
	(c)	$\|2^+\tilde{1}^+\tilde{1}1\rangle$	(Γ_5)
	(d)	$\|2^+\tilde{1}^+\tilde{1}\tilde{2}\rangle$	(Γ_4)
$^1G_4$	(a)	$\|4^+\tilde{1}^+\tilde{1}\tilde{2}\rangle$	(Γ_4)
	(b)	$0.3542\|4^+1^+11\rangle + 0.9352\|4^+\tilde{1}^+\tilde{1}1\rangle$	(Γ_5)
	(c)	$-0.1648\|4^+0^+00\rangle + 0.9863\|4^+2^+20\rangle$	(Γ_1)
	(d)	$\|4^+1^+1\tilde{0}\rangle$	(Γ_2)
	(e)	$\|4^+2^+22\rangle$	(Γ_3)
	(f)	$-0.9352\|4^+1^+11\rangle + 0.3542\|4^+\tilde{1}^+\tilde{1}1\rangle$	(Γ_5)
	(g)	$0.9863\|4^+0^+00\rangle + 0.1648\|4^+2^+20\rangle$	(Γ_1)
$^1D_2$	(a)	$\|2^+2^+20\rangle$	(Γ_1)
	(b)	$\|2^+\tilde{1}^+\tilde{1}1\rangle$	(Γ_5)
	(c)	$\|2^+\tilde{1}^+\tilde{1}\tilde{2}\rangle$	(Γ_4)
	(d)	$\|2^+2^+22\rangle$	(Γ_3)
$^1I_6$	(a)	$\|6^+2^+22\rangle$	(Γ_3)
	(b)	$-0.8228\|6^+\tilde{1}_0^+\tilde{1}\tilde{2}\rangle - 0.5684\|6^+\tilde{1}_1^+\tilde{1}\tilde{2}\rangle$	(Γ_4)
	(c)	$-0.3433\|6^+1^+11\rangle + 0.7753\|6^+\tilde{1}_0^+\tilde{1}1\rangle + 0.5302\|6^+\tilde{1}_1^+\tilde{1}1\rangle$	(Γ_5)
	(d)	$0.4142\|6^+0^+00\rangle + 0.9102\|6^+2^+20\rangle$	(Γ_1)
	(e)	$\|6^+\tilde{0}^+\tilde{0}2\rangle$	(Γ_3)
	(f)	$0.1411\|6^+1^+11\rangle + 0.6006\|6^+\tilde{1}_0^+\tilde{1}1\rangle - 0.7870\|6^+\tilde{1}_1^+\tilde{1}1\rangle$	(Γ_5)
	(g)	$\|6^+1^+1\tilde{0}\rangle$	(Γ_2)
	(h)	$-0.5684\|6^+\tilde{1}_0^+\tilde{1}\tilde{2}\rangle + 0.8228\|6^+\tilde{1}_1^+\tilde{1}\tilde{2}\rangle$	(Γ_4)
	(i)	$-0.9285\|6^+1^+11\rangle - 0.1954\|6^+\tilde{1}_0^+\tilde{1}1\rangle - 0.3156\|6^+\tilde{1}_1^+\tilde{1}1\rangle$	(Γ_5)
	(j)	$-0.9102\|6^+0^+00\rangle + 0.4142\|6^+2^+20\rangle$	(Γ_1)
$^3P_1$	(a)	$\|1^+1^+11\rangle$	(Γ_5)
	(b)	$\|1^+1^+1\tilde{0}\rangle$	(Γ_2)
$^3P_2$	(a)	$\|2^+2^+22\rangle$	(Γ_3)
	(b)	$\|2^+2^+20\rangle$	(Γ_1)
	(c)	$\|2^+\tilde{1}^+\tilde{1}1\rangle$	(Γ_5)
	(d)	$\|2^+\tilde{1}^+\tilde{1}\tilde{2}\rangle$	(Γ_4)

References

[1] Esterowitz L 1985 *Opt. Eng.* **29** 676
[2] Stoneman R C and Esterowitz L 1980 *Opt. Lett.* **15** 486
[3] Targ R, Kavaya M J, Huffaker R M and Bowles R L 1991 *Appl. Opt.* **30** 2013
[4] Cha S, Chan K P and Killinger D K 1992 *Appl. Opt.* **30** 189
[5] Saito H, Chaddha S, Chang R S F and Djeu N 1992 *Opt. Lett.* **17** 189
[6] Knoll K D 1971 *Phys. Status Solidi* b **45** 553
[7] Wortman D E, Leavitt R P and Morrison C A 1974 *J. Phys. Chem. Solids* **35** 591
[8] Kumar V, Vishwamittar and Chandra K 1977 *J. Phys. C: Solid State Phys.* **10** 267
[9] Ohta K, Saito H, Obara M and Djeu N 1993 *Japan. J. Appl. Phys.* **32** 1651
[10] Ohta K, Saito H and Obara M 1993 *J. Appl. Phys.* **73** 3149
[11] Henssen C H, Chaddha S, Shaw L B, Chang R S F, Djeu N and Saito H 1992 *Tech. Dig. Conf. on Laser and Electro-Optics (Anabeim, 1992)* (Washington, DC: Optical Society of America) paper CMD4
[12] Luo Zundu and Huang Yidong 1993 *J. Phys.: Condens. Matter* **5** 6949
[13] Luo Zundu and Huang Yidong 1994 *J. Phys.: Condens. Matter* **6** 3737
[14] Chen Xueyuan and Luo Zundu 1996 *J. Phys.: Condens. Matter* **8** 2571
[15] Chen Xueyuan and Luo Zundu 1997 *J. Phys.: Condens. Matter* **9** 1
[16] Butler P H 1981 *Point Group Symmetry Application: Method and Tables* (New York: Plenum)
[17] Pappalardo R 1976 *J. Lumin.* **14** 159
[18] Morrison C A and Leavitt R P 1979 *J. Chem. Phys.* **71** 2366
[19] Karayianis N 1971 *J. Chem. Phys.* **55** 3734
[20] Richards D B and Legvold S 1969 *Phys. Rev.* **186** 508
[21] Cooke A H, Swithenby S J and Wells M R 1972 *Solid State Commun.* **10** 265
[22] Lomheim T S and DeShazer L G 1978 *J. Appl. Phys.* **49** 5517
[23] Luo Zundu, Chen Xueyuan and Zhao Tingjie 1997 *Opt. Commun.* **134** 415
[24] Kuwano Y and Saito S 1990 *Rev. Laser Eng.* **18** 616 (in Japanese)
[25] Dexter D L 1953 *J. Chem. Phys.* **21** 836
[26] Freeman A J and Watson R E 1962 *Phys. Rev.* **127** 2058
[27] Chakoumakos B C, Abraham M M and Boatner L A 1994 *J. Solid State Chem.* **109** 197
[28] Inokuti M and Hirayama F 1965 *J. Chem. Phys.* **43** 1978